Progress in Organic Coatings 200 (2025) 109050

Contents lists available at ScienceDirect

Progress in Organic Coatings

journal homepage: www.elsevier.com/locate/porgcoat

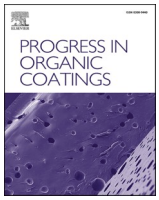

Functional group activation and coupling agent migration induced by plasma treatment in adhesive for enhanced toughness of metal-composite joints

Yongsoon Shin [a,*], Yao Qiao [a,1], Ethan K. Nickerson [a], Areesa A. Trevino [a], Mary Gilliam [b], Graham Garner [b], Michael Lukitsch [b], Blair E. Carlson [b], Kevin L. Simmons [a]

[a] Pacific Northwest National Laboratory, Richland, WA 99352, United States of America
[b] GM Global Technical Center-Research Scientific Building, 30470 Harley Earl Boulevard, Warren, MI 48092-2031, United States of America

ARTICLE INFO

Keywords:
Plasma
Migration
Activation
Adhesive
Double cantilever beam
Dissimilar joints

ABSTRACT

Commercial adhesive paste was additionally activated using low-power oxygen-containing plasma with different plasma exposure durations to investigate its interfacial bonding contribution in adhesively-bonded Aural-5/CFRP-PA6 double cantilever beam (DCB) joints with plasma-treated adherends. The plasma-treated adhesive showed enhanced functional peak intensities in Fourier transfer infrared spectroscopy (FTIR) as plasma exposure time was increased, and some degree of oxidation was also detected via X-ray photoelectron spectroscopy (XPS). A small molecule, dicyandiamide (coupling agent) in adhesive was migrated to adhesive layer, where double concentration of coupling agent was detected after 10 min of plasma treatment. As a result, characterization of the adhesive/CFRP-PA6 interface after DCB fracture showed additional chemical bonds formed through amine-initiated epoxy ring opening polymerization, as well as amide bonds and ester bonds. These additional bonds at the adhesive/CFRP-PA6 interfaces led to significantly increased failure extensions and fracture energies of the joints as the plasma exposure time on the adhesive increased, compared to the joints with plasma-treated adherends but non-plasma-treated adhesive as commonly seen in the literature.

1. Introduction

Assembling dissimilar materials, such as metal and carbon fiber-reinforced polymer (CFRP), has become an important topic in many industrial areas, including automotive and aerospace engineering [1,2]. Among various joining methods (i.e. rivets, adhesive, screws, welds, and others), adhesive bonding has become a promising approach in such fields [3]. The main advantages of adhesive bonding over the mechanical methods of riveting and bolting are the reduction in weight, the ease of joining dissimilar materials, the improvement in corrosion resistance, and the reduction of stress concentrations generated near holes used for mechanical assembly. Many efforts have been made to develop various types of adhesives for the bonding of dissimilar materials. However, joining quality and inconsistent failures in the interface of adhesively-bonded components have remained critical issues [4]. Manufacturing-induced defects and inconsistent surface treatment such as interfacial voids [5] and insufficient chemical bonding between adhesive and adherend, can cause the failure of adhesively-bonded structures.

On the other hand, various types of surface modification methods have been investigated to enhance the interfacial bonding strength of adhesively-bonded joints. These methods include chemical coating [6,7], plasma treatment [8,9], and laser treatment including surface patterning [10,11]. Among these methods, plasma treatment has been attracting more attention due to its quick, easy, and environmental friendly process. Polar functional groups such as -COOH, -OH, or -NH_2 were produced when air and N_2 were used as plasma gases [12–15]. These functional groups increase the surface energy of the adherend and enhance surface adhesion upon contacting the adhesive. In addition, how processing parameters such as treatment speed, working distance above the adherend's surface, and step-over distance used in plasma treatment affect a thermoplastic-based composite's surface and the fracture resistance of metal-composite dissimilar joints has also been studied in the literature [16,17]. Interestingly, while the plasma modification of adhesive surfaces alone on the bonding performance of a

* Corresponding author.
E-mail address: yongsoon.shin@pnnl.gov (Y. Shin).
[1] Equal contribution as first authors.

https://doi.org/10.1016/j.porgcoat.2024.109050
Received 31 October 2024; Received in revised form 12 December 2024; Accepted 31 December 2024
Available online 6 January 2025

bonded structure has been studied in the literature [18], the plasma modifications of both adherends and adhesive have been rarely explored but were recently reported in a publication for a metal-composite dissimilar joint [19]. In this publication, in addition to plasma-treated adherends, further modification of the adhesive surface with low-power plasma showed an enhanced composite/adhesive interfacial adhesion, leading to an additional 40 % improvement in single lap shear strength compared to that of plasma-treated adherends alone. The enhancement mechanism due to further plasma modification of the adhesive was explained by the primary contribution of the formation of denser interfacial chemical bonds.

However, a deeper and more detailed understanding of how low-power plasma treatment affects the adhesive's surface chemistry (e.g., the exposure of buried functionalities, the generation of new functional groups, and the migration of molecules within the adhesive), as well as its interaction with a plasma-treated adherend, is still lacking in the current literature but is important for maximizing interfacial bonding and its density between adhesive and adherend surfaces. In particular, studies or information on chemical migration within adhesives are limited. There are only a few reports for chemical migration within adhesives using ultrasonic vibration [20] and thermal curing [21–23]. For example, the high frequency impact of adhesive caused by ultrasonic vibration facilitated its penetration into the microgrooves on the metal surfaces, thereby enhancing mechanical anchoring [20]. The migration of low molecular weight cyclic polyester oligomer (cyclic polyesters) during the thermal curing of the polyurethane-based adhesives has been reported [21,22], which are widely used for food packaging applications. In addition, a structural model adhesive showed that there was an enrichment of coupling agent, dicyandiamide (DICY), at the interface between adhesive and steel joints [24], and the migration of coupling agent in epoxy model adhesive (N,N,N′,N′-Tetraglycidyl-4-4′-diaminodiphenylmethane (TGDDM) cured with a combination of two cross-linking agents: 4-4′-diaminodiphenylsulfone (DDS) and DICY) during curing process was detected [25]. The coupling agents were migrated to the interface and produced gas products, HCN, NH_3, and SO_2 without any oxidation. During the first stage of degradation, chain scission occurs by thermolysis. The thermally stable components are formed by molecular rearrangement, and the segments liberated by chain scission migrate to the surface and then either leave the sample as volatiles or are oxidized to gases by-products in the presence of oxygen [26]. Another example shows that silane coupling agents are used for glass surface improvement to minimize surface defects [27]. XPS results indicated that accelerated aging led to an increase in the concentration of hydroxyl groups resulting from the scission of amino silane crosslinking agents. The hydroxyl groups helped to migrate sodium ion from the glass substrate to the surface. Coupling agent-type amines forms hydrogen-bond surface complexes on an aluminum alloy (AA) surface due to the interaction of the amino group with surface hydroxyl groups by protonation of the amine termination (Al-OH…N bonds) or interaction with carbonaceous contamination ($C_xO_yH_z$ …N bonds) [28,29]. Bidentate diamines also form complexes with one amino group forming an O-Al…N bond and the other group forming an Al-OH…N or $C_xO_yH_z$ bond. The surface dissolved bidentate complexes, which are formed by ligand exchange between surface OH sites and the amino termination of the molecule, would be the precursor complexes of the interface in epoxy-amine/metal systems.

All the above enrichment detections of low molecular weight chemicals on the adhesive surface or in the interface of the adhesive and surface were activated by thermal curing. To date, to the best of the authors' knowledge, no study has reported on the migration of coupling agents through other methods, such as plasma surface modification of adhesives at room temperature, as investigated in this work.

The purpose of this work is to gain a deeper understanding of how low-power plasma with varying time durations influences the adhesive's surface (particularly the migration of coupling agents), its interaction with the adherend surface, and the resulting bonding performance. To this end, this work provides comprehensive results on understanding the surface activation and migration of coupling agents in the commercial epoxy adhesive Henkel EP 5089 through room temperature low-power oxygen-containing plasma treatment with varying exposure durations as shown in Fig. 1. Plasma-activated functional groups and increased coupling agent concentration were detected via FTIR and XPS on the surface layer of the adhesive relative to the non-plasma-treated adhesive surface. Moreover, the effects of those changes in surface chemistry of the adhesive, induced by different plasma exposure durations, on the enhanced fracture resistance of adhesively-bonded Aural-5/CFRP-PA6 dissimilar joints were evaluated by Double Cantilever Beam (DCB) tests, and their surface failure morphologies and modes were also characterized by an advanced profilometer.

2. Materials and methods

2.1. Materials

The thermoplastic composite investigated in this study was randomly distributed short carbon-fiber-reinforced polyamide 6 (CFRP-PA6) with a weight fraction of approximately 40 % fibers on average. Those composites were fabricated through injection molding and purchased from Teijin Automotive Technologies (Auburn Hills, MI USA). The die-cast Al adherend (Aural™-5: AA 374.1) was an aluminum alloy (AA) 374.1, purchased from Trialco Aluminum LLC (Chicago, IL USA). For simplicity, the name Aural-5 was used in this work to represent this metal. TEROSON EP 5089 adhesive product was provided by Henkel Corporation (Dűsseldorf, Germany). According to material safety data sheet (MSDS), the chemical composition of Henkel 5089 adhesive is shown in Table 1. The main components of Henkel 5089 are Bisphenol A-Epichlorohydrin polymer and Diglycidylether-bisphenol A (DGEBA). Filler and softeners were additionally added to control viscosity and processibility. Two phosphate (trixylyl phosphate and tris(methylphenyl) phosphate) are plasticizers to control viscosity of the adhesive. Calcium oxide and methyl ethyl ketone are filler and solvent. We found the coupling agent was dicyandiamide of about 1.0 wt% level.

2.2. Plasma treatments of adherends and adhesive

Two different plasma instruments were used to conduct plasma treatment of both adherend and adhesive. For the Aural-5 and CFRP-PA6 surfaces, a 500 W Blown-ion plasma system (Enercon Ind Co, Menomonee Falls, WA USA) with compressed air was used (Fig. 2a). In our recent publications [12,16], a combination of treatment parameters (i.e., nozzle tip end to surface distance (d), nozzle tip speed (v), step-over distance (so), and gas pressure (p)) using the same plasma system was reported to cause the highest improved surface energy on metal and CFRTP (carbon-fiber-reinforced thermoplastic polymer) surfaces, as well as enhanced interfacial bonding between CFRTP and adhesive. Accordingly, Aural-5 surface was treated using $d = 6.4$ mm, $v = 3.2$ mm/s, $so = 9$ mm, and $p = 85$ psi, whereas CFRP-PA6 surface was treated differently using a condition of $d = 3$ mm, $v = 100$ mm/s, $so = 9$ mm, and $p = 75$ psi. For Aural-5, the entire process took approximately 3.5 min to complete the treatment of the bonded area. For CFRP-PA6, the plasma treatment speed was much faster, thus only requiring approximately 7 s to complete the treatment of the bonded area. Regarding the surface temperatures of the adherends during the plasma treatment, for the investigated plasma processing parameters used in this work, the average surface temperatures during the plasma treatment were approximately 160 °C for the CFRP-PA6 adherend and 500 °C for the Aural-5 adherend. More details for measuring the surface temperature can be found in our previous publication [16]. On the other hand, the adhesive paste was first applied on plasma-treated Aural-5 surface and the adhesive surface was then plasma-treated using a low-power plasma cleaner with an adjustable radio frequency setting (Harrick Plasma, Ithaca, NY USA) (Fig. 2b). The adhesive paste was treated for 3, 6, and

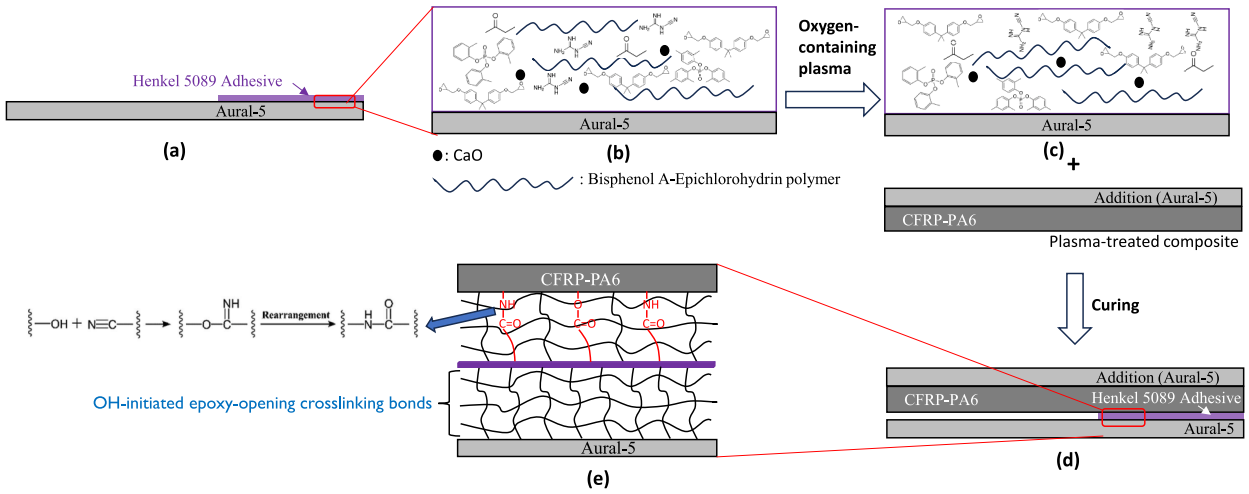

Fig. 1. Schematic illustration of the activation of adhesive by oxygen-containing plasma for enhanced interfacial bonding of adhesively-bonded Aural-5/CFRP-PA6 DCB joints. (a) Henkel EP 5089 adhesive applied on plasma-treated Aural-5, (b) adhesive layer containing epoxy polymers, fillers, and coupling agent (DICY), (c) activation of adhesive layer by oxygen-containing plasma, (d) curing of adhesively-bonded Aural-5/CFRP-PA6, and (e) additional interfacial bonds including amide and ester bonds (red) with migrated DICY on CFRP-PA6 surface. (For interpretation of the references to colour in this figure legend, the reader is referred to the web version of this article.)

Table 1
Components of Henkel 5089 epoxy adhesive paste.

Components	CAS no.	wt%
Bisphenol A-Epichlorohydrin polymer	25068-38-6	10–30
Diglycidylether-bisphenol A (DGEBA)	1675-54-3	10–30
Tris(methylphenyl) phosphate	1330-78-5	1–5
Calcium oxide	1305-78-8	1–5
Trixylyl phosphate	25155-23-1	0.1–1
Methyl ethyl ketone	78-93-3	0.1–0.3

10 min individually by using a gas mixture of 14 % oxygen and 86 % argon under ~300 m Torr and the power of 45 W (plasma working frequency: 13.56 MHz) with a gas flow of 20 mL/min.

2.3. Double cantilever beam (DCB) specimens' preparation and testing

Double Cantilever Beam (DCB) tests were conducted to investigate how additional plasma treatment on the adhesive, with varying time durations, affects the fracture resistance of Aural-5/CFRP-PA6 dissimilar joints. It is worth mentioning here that the investigated joint's configuration does not result in a pure mode I fracture but rather a mixed-mode fracture, with mode I fracture dominating over mode II fracture. However, the focus of this study mainly lies in explaining the chemical mechanisms of enhanced adhesive bonding rather than the accurate quantification of mode I fracture. To obtain a pure mode I fracture in bi-material adhesive joints, both flexural stiffness and strain distribution of adherends need to be taken into considerations as reported in the literature [30,31]. Both metal and CFRTP adherends have the same in-plane dimensions of 25.4 mm × 101.6 mm, but their thicknesses are different. The CFRP-PA6 adherend has a thickness of 3 mm, whereas the Aural-5 adherend has a thickness of 2 mm. Before conducting any plasma treatment, the surface of Aural-5 was wiped with acetone and cleaned using Scotch-Brite pads, whereas the CFRP-PA6 surface was left as-received. After conducting the plasma treatments on the adherends alone or both the adherends and adhesive, as described in Section 2.2, DCB specimens were prepared by adhesively bonding Aural-5 and CFRP-PA6 adherends with a bonded area of 25.4 mm × 38.2 mm. The same amount of the adhesive (0.22 mL) was used for each specimen to ensure consistent adhesive thickness. Strapping tape was applied along the edge of the adhesive bond line before curing to ensure a straight and uniform bond line, promoting consistent crack initiation [32]. Additionally, an extra Aural-5 adherend was bonded to the back side of the CFRP-PA6. This approach provides two benefits: (1) metal fixturing hinges for applying displacement can be bonded to the extra Aural-5 adherend, preventing adhesion failure between the CFRP-PA6 and the hinges, and (2) the extra Aural-5 adherend helps prevent bending fractures of the CFRTP during DCB testing. Finally, DCB specimens were cured in a conventional oven at 170 °C for 25 min with an average adhesive thickness of 50 μm. The details about DCB specimens are displayed in Fig. 2d.

In conducting the DCB tests, an ADMET 4200 load frame was used under displacement control with a displacement rate of 1.27 mm/min, following ASTM Standard D5528 for guidance. This load frame centers the specimen using opposing load forces, enabling Digital Image Correlation (DIC) analysis. The specimen sides were painted white with black speckles for DIC analysis, using the system from Correlated Solutions (Columbia, SC, USA). Three specimens were tested for each case to provide the data variation. In this work, the work of fracture method was used to calculate the ranges of specific fracture energies. These ranges were determined by assuming that unloading either goes to zero or remains parallel to the initial stiffness. More information on this method and the rationale for its use can be found in our recent publications [16,19].

2.4. Surface characterizations

The initial characterization involved assessing changes in the surface energy and wettability of the adhesive due to low-power oxygen-containing plasma treatment. Surface energy was determined by measuring the contact angles of water and diiodomethane drops on the adhesive surfaces using a KRÜSS mobile surface energy analyzer (MSA, KRÜSS Scientific Instruments, Matthews, NC, USA) and applying the Owens, Wendt, Rabel, and Kaelble (OWRK) method to calculate the polar and dispersive components of the adhesive's surface energy [12]. A MSA positional tool was placed to avoid touching the adhesive layer. After that, the wetting envelope of the adhesive can be further obtained, which represents the polar component as a function of the dispersive component for any contact showing zero contact angle [12].

FTIR spectroscopy was then employed, and the spectra of both the adherend and adhesive surfaces were collected using a Thermo Scientific NicoletTM iSTM 10 FTIR Spectrometer. The spectra were measured in the range of 4000–500 cm^{-1} with a resolution of 0.482 cm^{-1} and 128 scans were performed for each data point.

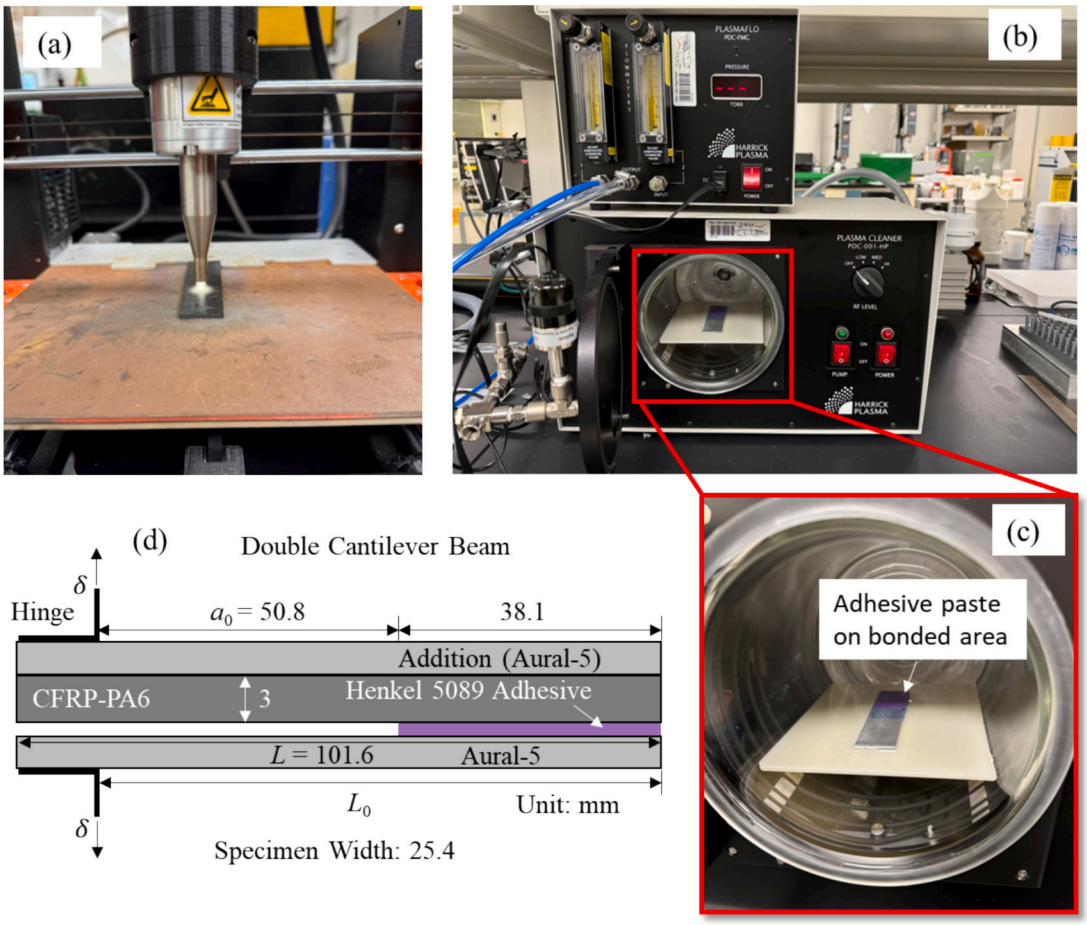

Fig. 2. (a) High-power (500 W) plasma treatment of adherends performed by a nozzle, (b) Low-power (45 W) plasma treatment of adhesive paste performed in a chamber, (c) Magnification of the specimen shown in b, and (d) DCB specimen configuration.

XPS measurements were further conducted on the adhesive using a Physical Electronics Quantera Scanning X-ray Microprobe (SXM). This system utilizes a focused monochromatic Al Kα X-ray source (1486.7 eV) for excitation and a spherical section analyzer. High energy resolution spectra were collected with a pass-energy of 69.0 eV and a step size of 0.125 eV. The binding energy (BE) scale is calibrated using the Cu 2p3/2 feature at 932.62 ± 0.05 eV and the Au 4f7/2 feature at 83.96 ± 0.05 eV. To minimize sample charging during analysis, low energy electrons at 1 eV and 20 μA, along with low energy Ar + ions, were employed. The binding energy was charge-corrected by referencing the primary C1s line at 284.8 eV. Quantification was performed using the Origin software for the analysis of the selected narrow scan spectra for each

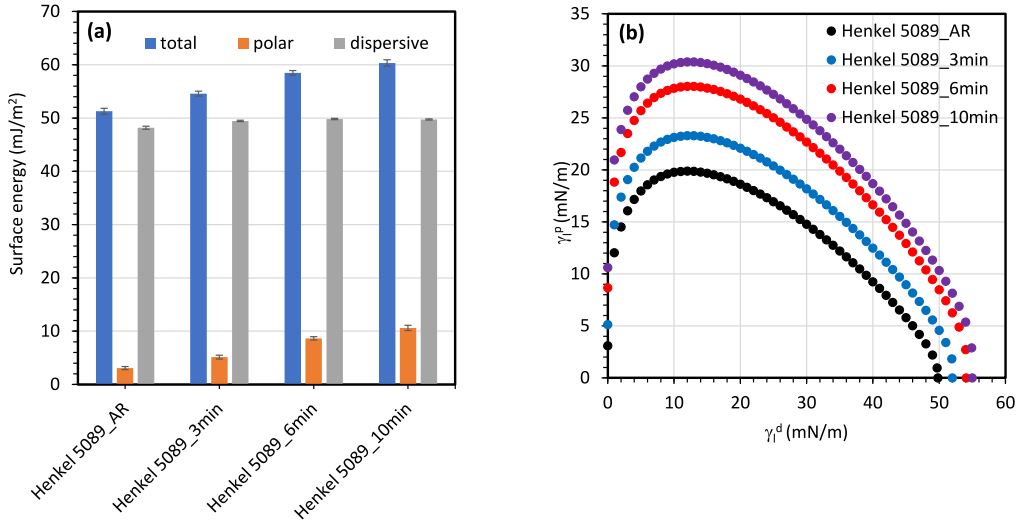

Fig. 3. Change in (a) surface energy and (b) wetting envelope of Henkel 5089 adhesive after oxygen-containing plasma treated with different time durations. Note, AR indicates as-received.

sample, which involved baseline correction and curve fitting.

The surface morphology of the separated adherends after DCB failure was visualized using a Keyence VR-5000 3D Optical Profilometer (Keyence Co., Itasca, IL, USA) to understand the failure modes and correlate them with the mechanical behavior of the joints. Approximately 70 sections of the bonded region were initially scanned at a magnification of 32×. The complete profile of the bonded area was then compiled by stitching these sections together.

3. Results and discussion

3.1. Effect of plasma treatment of adhesive on surface energy and wettability

Fig. 3 shows the change in surface energy and wetting envelope of Henkel 5089 adhesive after exposure to low-power plasma (14 % O_2/ 86% argon) with different time durations. Oxygen-containing plasma helped mainly to increase polar component, and the total surface energy of 17.7 % was increased after 10 min of oxygen-containing plasma exposure (Fig. 3a). Accordingly, the wetting envelope of the adhesive was enlarged as the oxygen-containing plasma exposure time increased, as shown in Fig. 3b. The foregoing results indicate the exposure of hydrophilic functionalities on the adhesive surface after low-power oxygen-containing plasma treatment as often reported in the literature [13,15,33].

In addition, whether any chemical migration from inside the adhesive to its surface occurs after plasma treatment requires further detailed characterization, which is sometimes overlooked in the literature, but it will be discussed in Sections 3.2 and 3.3. It is worth mentioning here that plasma exposure duration longer than 10 min was avoided for two reasons: (1) the surface energy of the adhesive was increased only slowly from 7 min to 10 min of plasma treatment, and the enhanced surface energy can be considered almost a maximum, and (2) some heat generation can occur after a longer plasma exposure time, which can lead to adhesive curing [13].

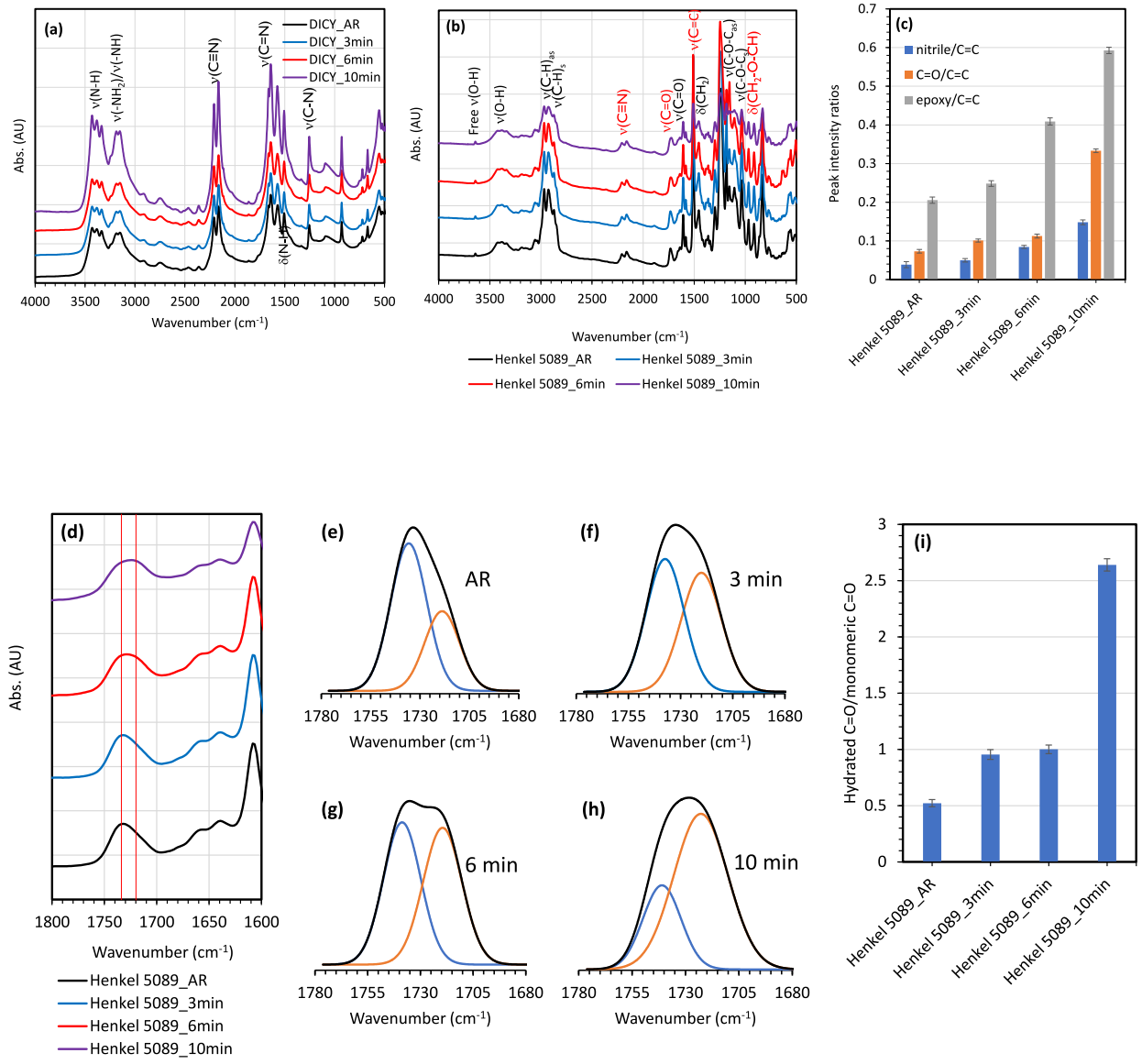

Fig. 4. FTIR spectra of low-power oxygen-containing plasma-treated (a) coupling agent, dicyandiamide (DICY), (b) Henkel 5089 adhesive, (c) change in intensity of characteristic peaks, (d) change in carbonyl peak, (e)-(h) deconvoluted carbonyl peak with respect to different plasma exposure durations, and (i) area ratios of hydrated (1725 cm^{-1}) to monomeric carbonyl peaks (1735 cm^{-1}) of oxygen-containing plasma treated Henkel 5089 adhesive.

3.2. Chemical analysis of plasma-treated adhesive: vibrational spectroscopy

FTIR spectra of Henkel 5089 activated by oxygen-containing plasma treatment were plotted in Fig. 4. First of all, coupling agent (DICY) was treated by the same oxygen-containing plasma (Fig. 4a), and found that no oxidation peaks including NO and NO_2, and degradation were observed. In oxygen-containing plasma treatment of adhesive, the spectra remained very similar even after 10 min of oxygen-containing plasma treatment without hardening or aging (no epoxy peak decrease) (Fig. 4b), but the ratios of several major peaks to C═C peak (1509 cm^{-1}) were significantly enhanced with increased plasma exposure time (Fig. 4c). These major peaks are located at 2159, 1727, and 913 cm^{-1}, representing nitrile, carbonyl, and epoxy, respectively. Interestingly, the nitrile group is part of the coupling agent, DICY, in the adhesive, indicating that DICY migrated to the adhesive surface due to the activation of oxygen-containing plasma.

On the other hand, it is important to investigate the change in carbonyl peak around 1720–1745 cm^{-1} (Fig. 4d), which can correlate to the plasma-activated carboxylate groups on the surface as often reported in the literature [12,16,34,35]. The carbonyl peak was changed as an increase of plasma treatment time due to the increase of hydrated C═O ratio around 1725 cm^{-1}. The deconvolution of each carbonyl peak showed an increased hydrated C═O relative to the monomeric C═O (1735 cm^{-1}) as an increase of plasma treatment time (Fig. 4d–i).

The increased peak ratios in Fig. 4c and i indicate that the low-power oxygen-containing plasma not only exposed carbonyl and epoxy groups on the adhesive surface, but also caused the migration of nitrile groups from within the adhesive to its surface. All of these functional groups on the adhesive surface contribute to the formation of interfacial bonds between the adhesive and the adherends, which will be discussed in detail in Section 3.5.

3.3. Chemical analysis of plasma-treated adhesive: X-ray photoelectron spectroscopy

Wide scan X-ray photoelectron spectra have been collected for as-received and three plasma treated adhesive specimens with different exposure durations to further understand surface composition changes, including the migration of DICY. Wide scan XPS spectra of Henkel adhesive show that those contain the species of C1s, O1s, N1s, Si2s, and Si2p, as shown in Fig. 5a. However, Si2s and Si2p were ignored because the adhesive was coated on Si wafer and exposed to oxygen-containing plasma for XPS measurement. The atomic composition as a function of oxygen-containing plasma exposure time was plotted in Fig. 5b. It is interesting to notice from this figure that the concentration of N1s gradually increased with longer exposure times, reaching about double the concentration compared to the as-received adhesive after 10 min of exposure. The O/C ratio after 10 min exposure was little lower than those of 3 and 6 min-exposed surfaces, and similar to that of the as-received adhesive surface because N was increased as shown in Fig. 5b. Please note that the ratios of nitrile, carbonyl, and epoxy in FTIR and the concentration changes of corresponding functionalities in XPS for the different plasma exposure durations can be different. This is caused by the difference of penetration depth of each energy source. FTIR typically provides information about bulk or thick surface (penetration depth: ~5–10 μm), but XPS primarily provides information of the first few atomic layers (penetration depth: ~ 5 nm) [36]. Therefore, all three functionalities are activated and increased in their concentration in adhesive (in FTIR) as an increase of plasma exposure durations as discussed in the previous section, but in XPS nitrogen concentration is dominantly increased on the adhesive surface. Because FTIR and XPS provide complementary information on chemical compositions of thin layer coating, their combination provides a powerful approach for studying the chemical composition in adhesive.

High resolution of the main elements C1s, O1s, and N1s of each surface with different oxygen-containing plasma exposure durations are shown in Fig. 6. The ratios of each atomic composition on the surface are collected in Table 2. In C1s spectra, Henkel 5089_AR showed two different peaks in as-received C1s spectrum: 54.3 % C—C and 45.7 % C—O at 284.80 and 286.50 eV. The latter peak showed an increase in C—O by 2.9 % after 3 min and 3.9 % after 6 min of oxygen-containing plasma treatment. However, after 10 min of plasma treatment, the C—O peak increased by only 1.0 %, and an additional 2.5 % of C═O was newly detected (Fig. 6a and Table 2). Unfortunately, C—N3 (289 eV) and C≡N (287 eV) of coupling agent DICY were not detected due to its small amount in C1s [37,38]. On the other hand, the O1s spectra showed similar patterns (Fig. 6b and Table 2). It remained the same after 6 min of plasma treatment, with only a C—O peak at 532.99 eV. However, after 10 min of plasma exposure, a new C═O peak at 531.93 eV appeared, constituting 14.1 % of the spectrum.

In the N1s spectra (Fig. 6c and Table 2), as-received adhesive showed only one peak of pyrrole-N (sp3 nitrogen: C-NH_2 and C2-NH) and -C ≡ N at 400 eV, which was maintained after 3 min of plasma treatment (Fig. 6c and Table 2). However, after 6 min of plasma exposure, the adhesive changed to 94.2 % of pyrrole-N and -C ≡ N at 400 eV and 5.8 % of pyridine-N (sp2 nitrogen: =NH and = N-) at 398.20 eV. The concentration of pyridine-N increased significantly to 17.6 % after 10 min of plasma treatment. The analysis of three major atoms in the adhesive indicates that there is no significant oxidation after 6 min of plasma exposure to the low-power oxygen-containing plasma, but it starts to oxidize further after 10 min of exposure. In addition, the as-received adhesive exposes pyrrole-N and nitrile groups on the surface, and the amount of pyridine-N on the surface increases slowly with longer plasma

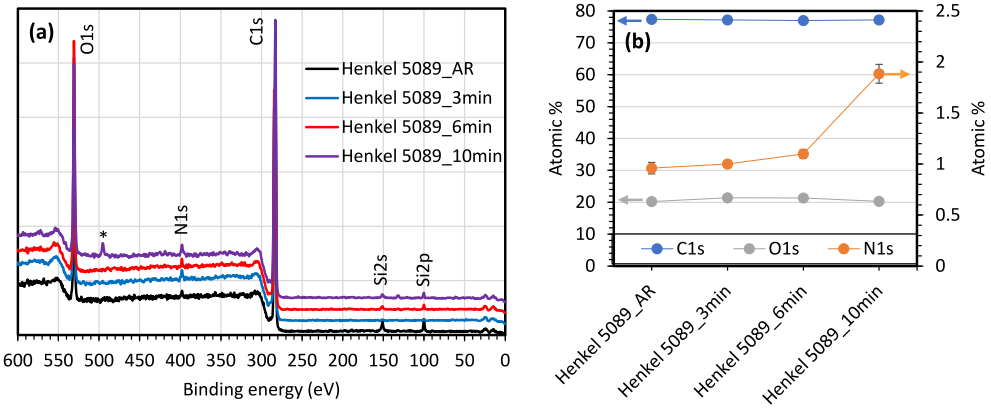

Fig. 5. (a) Wide scan XPS traces of as-received and oxygen-containing plasma-treated adhesive and (b) their atomic composition as a function of plasma treatment duration. Note, *Na impurity was detected (NaKLL) for 10 min of oxygen-containing plasma-treated adhesive.

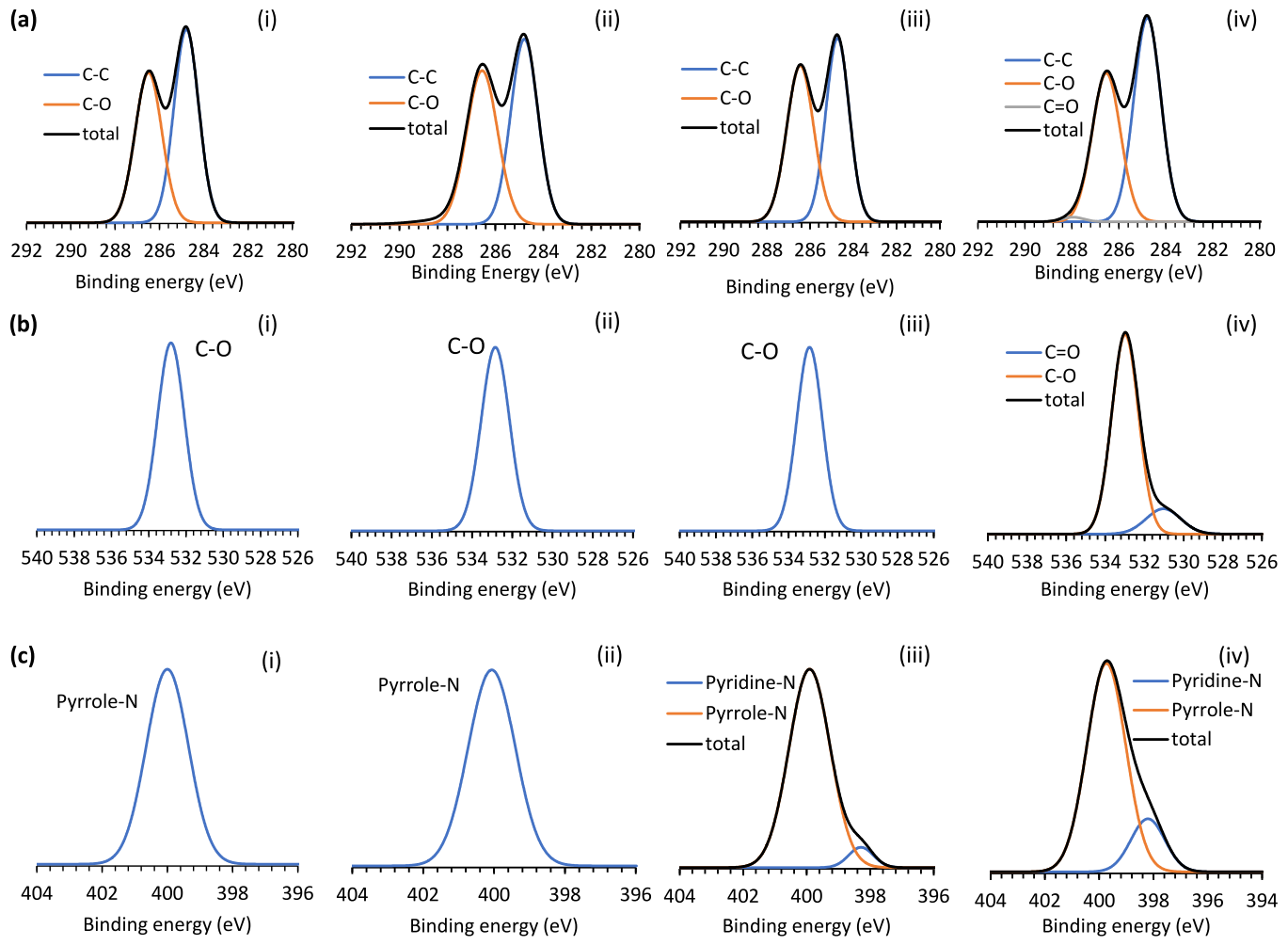

Fig. 6. High resolution (a) C1s, (b) O1s, and (c) N1s XPS analysis of (i) as-received, (ii) 3 min, (iii) 6 min, and (iv) 10 min oxygen-containing plasma-treated Henkel 5089 adhesive.

Table 2
Atomic composition (%) of as-received and plasma-treated Henkel 5089 adhesive.

Atom		Binding energy (eV)	As-received	3 min	6 min	10 min
C1s	C-C	284.80	54.3	51.4	50.4	51.0
	C-O	286.50	45.7	48.6	49.6	46.5
	C=O	287.96				2.5
O1s	C=O	531.93				14.1
	C-O	532.99	100.0	100.0	100.0	85.9
N1s	Pyridine-N	398.20			5.8	17.6
	Pyrrole-N	400.00	100.0	100.0	94.2	82.6

exposure time. This implies that the oxygen-containing plasma can cause the migration of small molecules or particles, such as DICY, to the surface, which helps form additional interfacial bonds between the adhesive and adherends. This aspect will be further discussed in Section 3.5.

3.4. Enhanced fracture energy of the joint due to additional plasma-treated adhesive

Having discussed the chemical changes on the adhesive surface due to the additional low-power oxygen-containing plasma treatment with varying exposure durations, the effects of these changes on the bonding performance of the joints were further evaluated in this section. As plotted in Fig. 7a, plasma treatments on the adherends or on both the adherends and adhesive did not noticeably increase the peak load in the load-displacement curves of the Aural-5/CFRP-PA6 joints, indicating no significant improvement in damage initiation within the joints. This aspect is reasonable, since the high stress concentration at the tip of the bond line within the joint always leads to rapid damage initiation, even when plasma surface modification is applied to improve the adhesive-adherend interfacial bonding, thus not enabling the measurement of the joint's strength improvement by plasma. However, a significant improvement was observed in the failure displacement with the application of plasma treatments, indicating a substantial enhancement in the fracture energy of the joint, since the DCB specimen was designed to measure the fracture energy due to its energy-driven crack propagation within the joint.

When high-power plasma treatments were applied on both metal and CFRTP adherends, the failure displacement was significantly increased as often reported in the literature [12,13,39,40]. More quantitatively, the average specific fracture energy ($\overline{G}_c$) of the joints with plasma-treated adherends exhibits an improvement of 51 %, showing a range of 2.1–3.0 N/mm compared to 1.4–2.0 N/mm for the as-received joints (Fig. 7b). When the adhesive was additionally treated with low-power oxygen-containing plasma, the failure displacement of the joint increased with longer plasma exposure durations, showing a particularly remarkable improvement after 10 min of oxygen-containing plasma exposure. In terms of the $\overline{G}_c$ value (Fig. 7b), the additional low-power

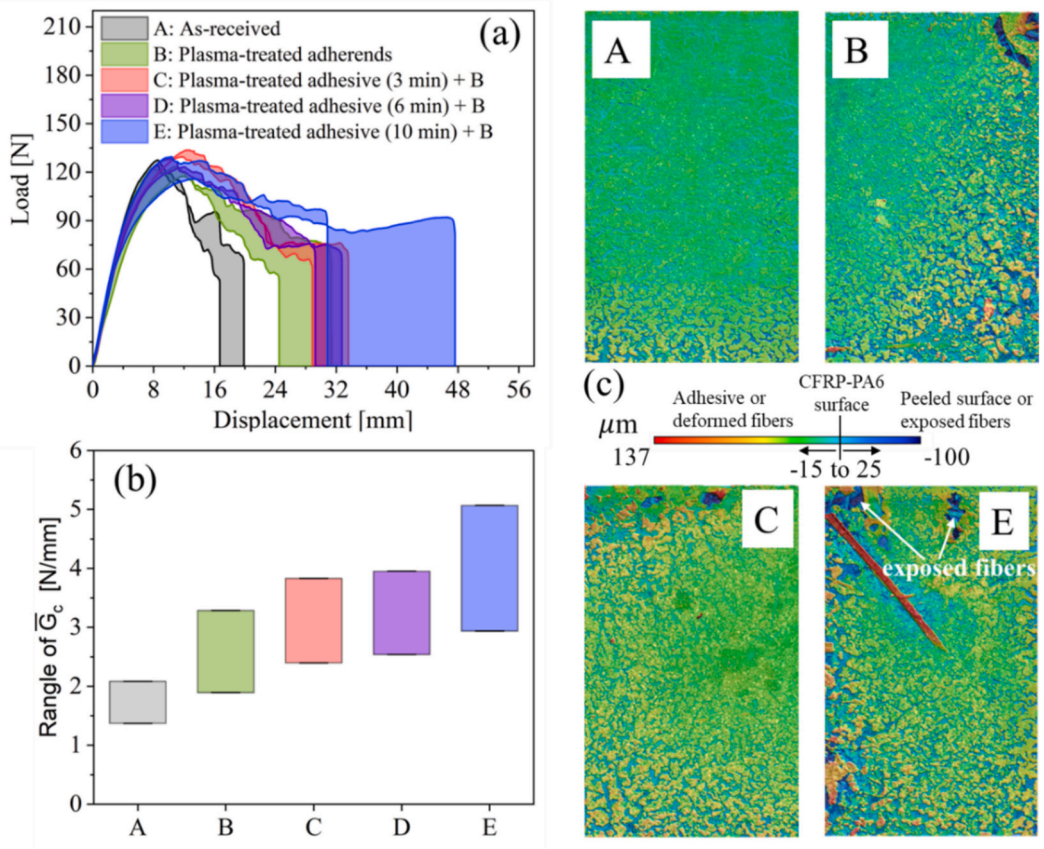

Fig. 7. (a) Load-displacement curves obtained from DCB tests for Aural-5/CFRP-PA6 joints under five different scenarios: (A) As-received adherends, (B) High-power plasma-treated adherends, (C-E) High-power plasma-treated adherends with low-power plasma-treated adhesive for 3 min, 6 min, and 10 min, respectively. (b) Range of $\overline{G}_c$ values for scenarios (A–E) as shown in (a). (c) Surface morphologies of CFRP-PA6 adherends after DCB failure for scenarios (A, B, C, and E) as mentioned in (a).

plasma treatment on the adhesive increased the $\overline{G}_c$ value to 2.5–3.6 N/mm (83 % improvement) for 3 min of plasma exposure, 2.6–3.9 N/mm (94 % improvement) for 6 min of plasma exposure, and up to 3.0–4.8 N/mm (144 % improvement) for 10 min of plasma exposure. It is worth mentioning that the measured fracture energy does not solely represent the adherend-adhesive interfacial fracture energy, as failure occurs in mixed modes, which will be discussed in the next paragraph. To obtain the true adherend-adhesive interfacial fracture energy, computational modeling can be used to calibrate the interfacial properties by matching experimental data with simulations, which is beyond the scope of this work.

The failure morphology of the CFRP-PA6 adherend surface after final separation of the joint supports the enhanced fracture resistance of the Aural-5/CFRP-PA6 joints. As illustrated in Fig. 7c, for as-received joints, damage occurred either very close to the CFRP-PA6 surface or at the CFRP-PA6/adhesive interface. For plasma-treated adherends alone, damage began to occur away from the CFRP-PA6/adhesive interface in some locations, as indicated by case B in Fig. 7c, which shows increased surface height of CFRP-PA6 after DCB failure. With additional low-power oxygen-containing plasma treatment on the adhesive, damage mainly propagated away from the CFRP-PA6/adhesive interface, as shown in cases C and F in Fig. 7c. Furthermore, as plasma exposure time on the adhesive increased, the surface layer deformed and/or peeled off, as exemplified by case E (10 min plasma exposure) in Fig. 7c. The surface failure morphologies of CFRP-PA6 adherends from plasma-treated joints clearly show more damage occurring within the adhesive (often termed cohesive failure) and the composite surface layer. These failure modes not only lead to increased dissipation of fracture energy, but also promote additional plastic bending of the Aural-5 adherend, thus further dissipating energy and thereby improving the bonding performance of the joints, as shown in Fig. 7a and discussed earlier in this section.

3.5. Interfacial bonds between adhesive and CFRP-PA6

The mechanism for enhanced fracture resistance of the Aural-5/CFRP-PA6 dissimilar joints due to the additional low-power oxygen-containing plasma on the adhesive was further explored via ATR-FTIR analysis. In a typical metal-CFRTP dissimilar joint, the key factors governing its bonding performance lie at the interfacial region between adhesive and CFRTP due to its weaker chemical bonding compared to that of adhesive and metal [12,16,41,42]. Thus, the failure surface of CFRP-PA6 adherend after the separation of the joint was chemically characterized using ATR-FTIR. To understand the chemical bonding at or very close to the interface of the adhesive and CFRP-PA6, the thickness of the remaining adhesive layer on the CFRP-PA6 surface needs to be minimized [28]. This was achieved by using a blade to carefully remove the adhesive layer as thin as possible until a small N—H stretching band of the CFRP-PA66 surface appeared at 3310 cm^{-1}, where ATR-FTIR spectra would be very close to the interfacial bonds on a similar level of average surface roughness of CFRP-PA6 (~10 μm). At that point, all measured ATR-FTIR spectra showed consistent chemical bonds at the interfacial region between the adhesive and CFRP-PA6 as shown in Fig. 8a.

Interestingly, the cured adhesive contained two carbonyl stretches (ν(C=O)$_{ester}$, ν(C=O)$_{amide}$), and epoxy bending (δ(CH_2-O-CH)) bands at 1735, 1638, and 916 cm^{-1}, respectively. Both ester and amide peaks in the cured adhesive are from urethane ester molecules formed by the reaction with a 2-imidooxazolidine with adhesive chains in amine-

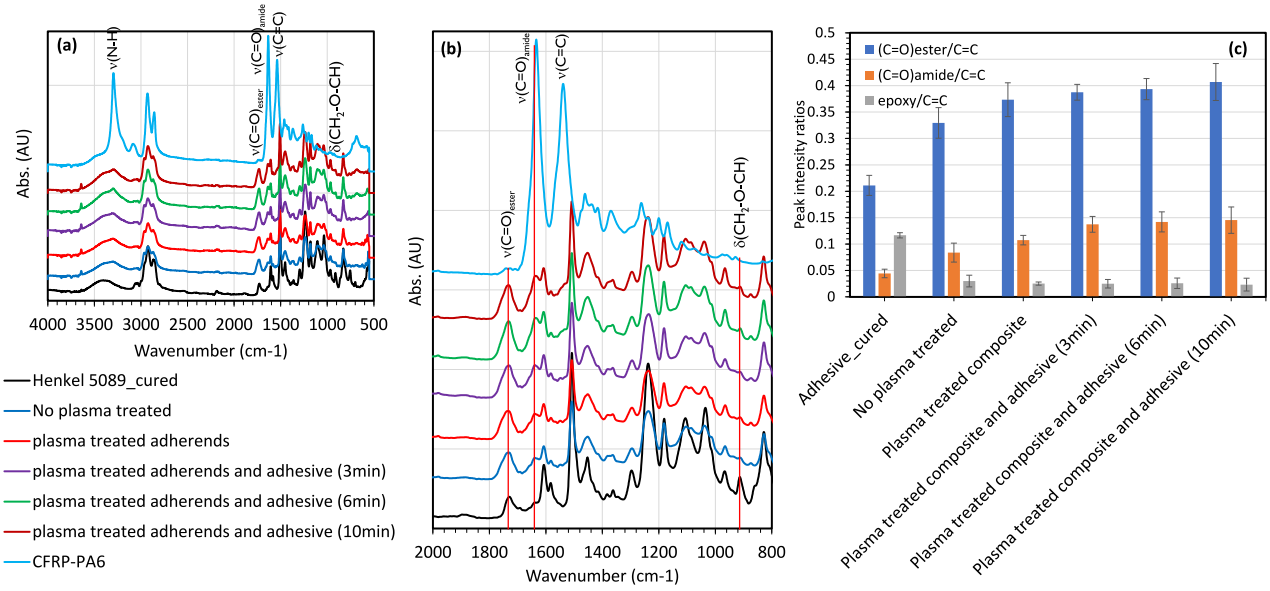

Fig. 8. (a) and (b) ATR-FTIR spectra of Aural-5 surfaces after the separation of the DCB joints, and (c) relative peak intensity ratios of $(C{=}O)_{ester}$, $(C{=}O)_{amide}$, and epoxy to (C=C).

initiated epoxy ring opening polymerization of epoxy adhesive [43,44]. Their peak intensity ratios relative to stable C=C stretching (at 1509 cm^{-1}) changed with different plasma exposure durations (Fig. 8b and c). More specifically, both C=O intensity ratios increased with longer plasma exposure but epoxy peak intensity ratio was decreased. This observation indicates that plasma treatment of adhesive can activate its functional groups on the surface, migrate the coupling agent to the surface, and oxidize adhesive layer. Therefore, in addition to the hydroxyl-initiated epoxy ring opening polymerization (by reaction hydroxyl groups on the CFRP-PA6 and epoxy rings on the adhesive) as well as inter-molecular hydrogen bonds at the CFRP-PA6/adhesive interface regardless of whether the adherends are as-received or high-power plasma-treated [18], as the time duration of the low-power oxygen-containing plasma on the adhesive increased, the following additional chemical bonds at the interfacial region between the adhesive and CFRP-PA6 were formed: (1) amine-initiated epoxy ring opening polymerization (by migration of coupling agent, in fact, it is the reaction between amino groups of coupling agent and adhesive, so that it is very close to interfacial bonding); (2) amide bonds (by reaction of hydroxyls on the CFRP-PA6 and nitrile groups of migrated coupling agent), and (3) ester bonds (by reaction of hydroxyls on the adhesive and carboxylic acids on the CFRP-PA6). Those results can also be supported by and consistent with ATR-FTIR of plasma-treated adhesive before being applied on the adherends (Fig. 4), where the enhanced amount of nitrile and epoxy groups on the adhesive by low-power oxygen-containing plasma mainly contributes to additional interfacial bonding formation.

4. Conclusions

In adhesively-bonded Aural-5/CFRP-PA6 dissimilar DCB joints, in addition to the commonly studied plasma-treated adherends, the commercial epoxy-based adhesive paste was also treated using low-power oxygen-containing plasma (14 % O_2/86% Ar). This additional plasma treatment of the adhesive led to the following conclusions:

1. About 17.7 % of the adhesive's surface energy (mostly polar component) was increased, and more C=O, C≡N, and epoxy peaks were exposed to the adhesive surface layer in ATR-FTIR spectra after 10 min of plasma treatment.
2. XPS showed that oxidation of adhesive was not detected after 6 min of exposure to the low-power oxygen-containing plasma, but some level of oxidation and the migration of coupling agent to the adhesive surface were detected after 10 min of plasma exposure.
3. As the duration of additional low-power oxygen-containing plasma treatment on the adhesive increased, Aural-5/CFRP-PA6 DCB joints exhibited further improvement in failure displacement. Accordingly, the highest enhanced $\overline{G}_c$ can reach up to 3–4.8 N/mm, being 61 % higher than that of the joints with plasma-treated adherends alone (2.1–3 N/mm) and 144 % higher than that of the as-received joints (1.4–2 N/mm).
4. The surface morphology of CFRP-PA6 after DCB failure confirmed the enhanced fracture resistance of the joints due to the additional oxygen-containing plasma treatment of the adhesive. This is evidenced by increased cohesive failure in the adhesive occurring away from the CFRP-PA6/adhesive interface and a small amount of peeling of the composite surface layer as the exposure time increases.
5. ATR-FTIR spectra were measured on the fracture surfaces of CFRP-PA6 after DCB failure, which explained that the enhanced joint's fracture resistance, achieved through the additional oxygen-containing plasma treatment of the adhesive, was due to the contribution of additional chemical bonds from amine-initiated epoxy ring opening polymerization, amides, and esters at the interfacial region between the adhesive and CFRP-PA6.

The proposed approach for the plasma treatment of adhesive paste, in addition to the common plasma treatment of adherends, is expected to be effective for metal-CFRTP dissimilar joints in general, extending beyond the investigated Aural-5/CFRP-PA6 combination.

CRediT authorship contribution statement

Yongsoon Shin: Writing – original draft, Methodology, Investigation, Formal analysis, Data curation, Conceptualization. **Yao Qiao:** Writing – review & editing, Investigation, Formal analysis, Conceptualization. **Ethan K. Nickerson:** Formal analysis. **Areesa A. Trevino:** Investigation. **Mary Gilliam:** Writing – review & editing, Funding acquisition. **Graham Garner:** Resources, Methodology. **Michael Lukitsch:** Writing – review & editing. **Blair E. Carlson:** Writing – review & editing, Supervision, Funding acquisition. **Kevin L. Simmons:** Supervision, Project administration, Funding acquisition.

Declaration of competing interest

The authors declare that they have no known competing financial interests or personal relationships that could have appeared to influence the work reported in this paper.

Acknowledgements

This work is supported by U.S. Department of Energy, Office of Energy Efficiency and Renewable Energy, Vehicle Technologies Office (EERE-VTO). PNNL is operated by Battelle Memorial Institute for the U. S. DOE under contract DE-AC 06-76RLO 1830. Authors would also like to thank Henkel Chemical Co. for providing their adhesives for this project.

Data availability

No data was used for the research described in the article.

References

[1] B.M. Nagarajan, M. Manoharan, Assessment of dissimilar joining between metal and polymer hybrid structure with different joining processes, J. Thermoplast. Compos. Mater. 36 (2023) 2169–2211, https://doi.org/10.1177/08927057211048534.
[2] S. Han, X. Guang, Z. Li, Y. Li, Joining processes of CFRP-Al sheets in automobile lightweighting technologies: a review, Polym. Compos. 43 (2022) 8622–8633, https://doi.org/10.1002/pc.27088.
[3] C. Cui, W. Liu, Recent advances in wet adhesives: adhesion mechanism, design principle and applications, Prog. Polym. Sci. 116 (2021) 101388, https://doi.org/10.1016/j.progpolymsci.2021.101388.
[4] A.Y. Kanani, S. Green, X. Hou, J. Ye, Hybrid and adhesively bonded joints with dissimilar adherends: a critical review, J. Adhes. Sci. Technol. 35 (2021) 1821–1859, https://doi.org/10.1080/01694243.2020.1861859.
[5] Y. Qiao, S. Ko, A. Samanta, D.R. Merkel, Y. Shin, A. Guzman, E.K. Nickerson, J. L. Ramos, K.L. Simmons, A micro-scale numerical investigation of internal and interfacial void defects in adhesive on failure behavior of adhesively-bonded bi-materials with rough surfaces, in: Proceeding of the American Society of Mechanical Engineers (ASME) - 1st Annual Aerospace Structures, Structural Dynamics, and Materials (SSDM) Conference, 2023, https://doi.org/10.1115/SSDM2023-105653 (New Orleans, LA).
[6] J. Shi, H. Pries, E. Stammen, K. Dilger, Chemical pretreatment and adhesive bonding properties of high-pressure die cast aluminum alloy: AlSi10MnMg, Inter. J. Adhes. Adhes. 61 (2015) 112–121, https://doi.org/10.1016/j.ijadhadh.2015.06.002.
[7] J. Nagel, M. Bräuer, B. Hupfer, K. Grundke, S. Schwarz, D. Lehmann, Investigations on the reactive surface modification of polycarbonate by surface-reactive injection molding, J. Appl. Polym. Sci. 93 (2004) 1186–1191, https://doi.org/10.1002/app.20577.
[8] K. Takenaka, A. Jinda, S. Nakamoto, R. Koyari, S. Toko, G. Uchida, Y. Setsuhara, Influence of pre-treatment using non-thermal atmospheric pressure plasma jet on aluminum alloy A1050 to PEEK direct joining with hot-pressing process, Inter. J. Adv. Manuf. Technol. 130 (2024) 1925–1933, https://doi.org/10.1007/s00170-023-12827-7.
[9] B. Jiang, Q. Chen, J. Yang, Advances in joining technology of carbon fiber-reinforced thermoplastic composite materials and aluminum alloys, Inter. J. Adv. Manuf. Technol. 110 (2020) 2631–2649, https://doi.org/10.1007/s00170-020-06021-2.
[10] H.M. Meyer III, A.S. Sabau, C. Daniel, Surface chemistry and composition-induced variation of laser interference-based surface treatment of Al alloys, Appl. Surf. Sci. 489 (2019) 893–904, https://doi.org/10.1016/j.apsusc.2019.06.001.
[11] S. Tofil, R. Barbucha, M. Kocik, R. Kozera, M. Tanski, N. Arivazhagan, J. Yao, A. Zrak, Adhesive joints with laser shaped surface microstructures, Materials 14 (2021) 7548, https://doi.org/10.3390/ma14247548.
[12] Y. Shin, Y. Qiao, N. Canfield, Z. Yu, H.M. Meyer III, D.R. Merkel, E.K. Nickerson, N. S. Kanbargi, A. Ortiz, A.K. Naskar, K.L. Simmons, Significant slowdown of plasma-optimized surface energy deactivation by vacuum sealing for efficient adhesive bonding, Compos. B Eng. 240 (2022) 110001, https://doi.org/10.1016/j.compositesb.2022.110001.
[13] J. Lin, C. Sun, J. Min, H. Wan, S. Wang, Effect of atmospheric pressure plasma treatment on surface physicochemical properties of carbon fiber reinforced polymer and its interfacial bonding strength with adhesive, Compos. B Eng. 199 (2020) 108237, https://doi.org/10.1016/j.compositesb.2020.108237.
[14] A. Nandi, A.K. Biswal, A. Nguyen, L. Nordyke, E. Behling, T. Foulds, K. Schultz, A. Vashisth, Comparative study of surface preparation for paint adhesion on CF-PEKK composites: plasma, chemical, and flame treatment, Appl. Surf. Sci. 669 (2023) 160533, https://doi.org/10.1016/j.apsusc.2024.160533.
[15] Y. Qiao, Y. Shin, M.R. Pallaka, E.K. Nickerson, L.D. Fring, S. Ko, J.L. Ramos, H. F. Wu, K.L. Simmons, Polymer-fiber-reinforced polymers with enhanced interfacial bonding between polypropylene fiber and polyethylene matrix, J. Reinf. Plast. Comp. (2024), https://doi.org/10.1177/07316844241281127 (in press).
[16] Y. Qiao, Y. Shin, M.R. Pallaka, E.K. Nickerson, D.R. Merkel, R.J. Seffens, A. Ortiz, J. L. Ramos, K.L. Simmons, Plasma surface modification coupled with thermal and step-over distance effects on significant fracture improvement of adhesively-bonded metal-CFRTP dissimilar materials, Compos. Sci. Technol. 232 (2023) 109833, https://doi.org/10.1016/j.compscitech.2022.109833.
[17] C. Sun, J. Min, J. Lin, H. Wan, Effect of atmospheric pressure plasma treatment on adhesive bonding of carbon fiber reinforced polymer, Polymers 11 (2019) 139, https://doi.org/10.3390/polym11010139.
[18] M. Kawabe, S. Tasaka, N. Inagaki, Effects of surface modification by oxygen plasma on peel adhesion of pressure-sensitive adhesive tapes, J. Appl. Polym. Sci. 78 (2000) 1392–1401, https://doi.org/10.1002/1097-4628(20001114)78:7<1392::AID-APP100>3.0.CO;2-U.
[19] Y. Qiao, Y. Shin, J.R. Ramos, M.H. Engelhard, R.J. Seffens, D.R. Merkel, K. L. Simmons, Plasma treatment on both adhesive tape and adherends for significantly enhanced CFRTP-related adhesive joints, Appl. Surf. Sci. 649 (2024) 159092, https://doi.org/10.1016/j.apsusc.2023.159092.
[20] Y. Wang, H. Wang, Y. Chen, W. Zhou, L. Hua, Adhesion improvement and strengthening mechanisms of ultrasonic adhesive-impact bonding process for CFRP/Ni bonded joints, Surf. Interfaces 46 (2024) 104108, https://doi.org/10.1016/j.surfin.2024.104108.
[21] N. Zhang, G. Kenion, D. Bankmann, S. Mezouari, T.G. Hartman, Migration studies and chemical characterization of low molecular weight cyclic polyester oligomers from food packaging lamination adhesives, Packag. Technol. Sci. 31 (2018) 197–211, https://doi.org/10.1002/pts.2367.
[22] S. Ubeda, M. Aznar, A.K. Rosenmai, A.M. Vinggaard, C. Nerin, Migration studies and toxicity evaluation of cyclic polyesters oligomers from food packaging adhesives, Food Chem. 311 (2020) 125918, https://doi.org/10.1016/j.foodchem.2019.125918.
[23] E. Belov, K. Nadaraia, I. Imshinetskiy, D. Mashtalyar, L. Ignatieva, Y. Marchenko, I. Osmushko, M. Gerasimenko, S. Sinebruykhov, S. Gnedenkov, Polymer system based on polyethylene glycol and TFE telomers for producing films with switchable wettability, Int. J. Mol. Sci. 25 (2024) 4904, https://doi.org/10.3390/ijms25094904.
[24] B. De'Neve, M. Delamar, T.T. Nguyen, M.E.R. Shanahan, Failure mode and ageing of steelrepoxy joints, Appl. Surf. Sci. 134 (1998) 202–212, https://doi.org/10.1016/S0169-4332(98)00220-7.
[25] X. Buch, M.E.R. Shanahan, Migration of cross-linking agents to the surface during ageing of a structural epoxy adhesive, Inter. J. Adhes. Adhes. 32 (2003) 261–267, https://doi.org/10.1016/S0143-7496(03)00028-9.
[26] X. Buch, M.E.R. Shanahan, Thermal and thermo-oxidative ageing of an epoxy adhesive, Polym. Degrad. Stab. 68 (2000) 403–411, https://doi.org/10.1016/S0141-3910(00)00028-8.
[27] B.R. Whittle, R.J. Hand, B. Ellis, J.D. Whittle, R.D. Short, The effect of a silane coupling agent on the hydrolytic durability of thin epoxy resin films, J. Adhes. 77 (2001) 1–24, https://doi.org/10.1080/00218460108030729.
[28] D. Mercier, J.-C. Rouchaud, M.-G. Barthe's-Labrousse, Interaction of amines with native aluminum oxide layers in non-aqueous environment: application to the understanding of the formation of epoxy-amine/metal interphases, Appl. Surf. Sci. 254 (2008) 6495–6503, https://doi.org/10.1016/j.apsusc.2008.04.010.
[29] M.-G. Barthe's-Labrousse, Mechanisms of formation of the interphase in epoxy-amine/aluminum joints, J. Adhes. 88 (2012) 699–719, https://doi.org/10.1080/00218464.2012.682933.
[30] W. Wang, R.L. Fernandes, S.T. De Freitas, D. Zarouchas, R. Benedictus, How pure mode I can be obtained in bi-material bonded DCB joints: a longitudinal strain-based criterion, Compos. B Eng. 153 (2018) 137–148, https://doi.org/10.1016/j.compositesb.2018.07.033.
[31] W. Wang, S.T. De Freitas, J.A. Poulis, D. Zarouchas, A review of experimental and theoretical fracture characterization of bi-material bonded joints, Compos. B Eng. 206 (2021) 108537, https://doi.org/10.1016/j.compositesb.2020.108537.
[32] Y. Qiao, D.R. Merkel, E.K. Nickerson, Y. Shin, R.J. Seffens, A. Ortiz, K.L. Simmons, Mode I tensile fracture behavior of adhesively-bonded metal-metal, metal-CFRP, CFRP-CFRP bi-material combinations analyzed by size effect method, Compos. Part A-Appl. S. (2022) 107025, https://doi.org/10.1016/j.compositesa.2022.107025.
[33] Y. Shin, Y. Qiao, N. Yelin, J.L. Ramos, E.K. Nickerson, D.R. Merkel, K.L. Simmons, Interfacial bond characterization of epoxy adhesives to aluminum alloy and carbon fiber-reinforced polyamide by vibrational spectroscopy, Surf. Interfaces 42 (2023) 103346, https://doi.org/10.1016/j.surfin.2023.103346.
[34] F. Moroni, F. Musiari, C. Sciancalepore, M. Messori, Influence of atmospheric pressure plasma process parameters on the mechanical behavior of thermoplastic joints, Inter. J. Adhes. Adhes. 102 (2020) 102650, https://doi.org/10.1016/j.ijadhadh.2020.102650.
[35] Y. Qiao, Y. Shin, E.K. Nickerson, D.R. Merkel, A. Ortiz, K.L. Simmons, Adhesively-bonded Metal-CFRTP bi-materials: enhanced crack growth resistance via plasma and quantified fracture via size effect method, in: Proceeding of the American Society for Composites (ASC) 37th Annual Technical Conference, 2022, https://doi.org/10.12783/asc37/36496 (Tucson, AR).
[36] R. Morent, N. De Geyter, C. Leys, L. Gengembre, E. Payen, Comparison between XPS- and FTIR-analysis of plasma-treated polypropylene film surfaces, Surf. Interface Anal. 40 (2008) 597–600, https://doi.org/10.1002/sia.2619.
[37] G. Säckl, J. Duchoslav, R. Pugstaller, C. Marchfelder, K. Haselgrübler, M. Aufray, D. Stifter, G.M. Wallner, The interaction of waterborne epoxy/dicyandiamide varnishes with metal oxides, Polymers 14 (2022) 2226, https://doi.org/10.3390/polym14112226.

[38] G. Beamson, D. Briggs, The XPS of Polymers Database: Surface Spectra, First ed., Manchester, UK, 2000.
[39] Y. Qiao, E.K. Nickerson, T.J. Roosendaal, J.L. Ramos, K.L. Simmons, Effects of air plasma treatment with gradient speeds on fracture of adhesively-bonded metal-CFRTP dissimilar joints, SAMPE Conference (North America Society for the Advancement of Material and Process Engineering) (2023), https://doi.org/10.33599/nasampe/s.23.0014.
[40] C. Yildirim, H. Ulus, B. Beylergil, A. Al-Nadhari, S. Topal, M. Yildiz, Effect of atmospheric plasma treatment on mode-I and mode-II fracture toughness properties of adhesively bonded carbon fiber/PEKK composite joints, Eng. Fract. Mech. 289 (2023) 109463, https://doi.org/10.1016/j.engfracmech.2023.109463.
[41] Y. Qiao, R.J. Seffens, E.K. Nickerson, T.J. Roosendaal, D.R. Merkel, Y. Shin, J. L. Ramos, S. Ko, A. Samanta, M.R. Pallaka, A. Ortiz, K.L. Simmons, A study of adhesive bonding in metal-metal, metal-CFRP, and CFRP-CFRP material combinations under shear deformation: fracture morphologies and damage mechanisms, Inter. J. Adhes. Adhes. 127 (2023) 103511, https://doi.org/10.1016/j.ijadhadh.2023.103511.
[42] Y. Qiao, D.R. Merkel, E.K. Nickerson, R.J. Seffens, Y. Shin, M.R. Pallaka, J. L. Ramos, A. Ortiz, K.L. Simmons, The roles of interface, adherend, and adhesive in plasma-and other-treated joints of metals and FRP materials under shear deformation, in: The American Society for Composites (ASC) 37th Annual Technical Conference, 2022, https://doi.org/10.12783/asc37/36378 (Tucson, Arizona).
[43] F. Wu, X. Zhou, X. Yu, Reaction mechanism, cure behavior and properties of a multifunctional epoxy resin, TGDDM, with latent curing agent dicyandiamide, RSC Adv. 8 (2018) 8248, https://doi.org/10.1039/c7ra13233f.
[44] M.-F. Grenier-Loustalot, M.-P. Bente, P. Grenier, Reactivite du dicyandiamide vis a vis des groupements O et N-epoxyde-1, Mecanisme reactionnel. Eur. Polym. J. 27 (1991) 1201–1216, https://doi.org/10.1016/0014-3057(91)90057-U.